Dispersion of Silicate in Tricalcium Phosphate Elucidated by Solid-State NMR

A. Rawal,[†] X. Wei,[‡] M. Akinc,[‡] and K. Schmidt-Rohr*,[†]

Department of Chemistry and Department of Materials Science and Engineering, Iowa State University and Ames Laboratory, Ames, Iowa 50011

Received October 10, 2007. Revised Manuscript Received January 19, 2008

The dispersion of silicate in tricalcium phosphate, a resorbable bioceramics for bone replacement, has been investigated by various solid-state nuclear magnetic resonance (NMR) methods. In samples prepared with 5 and 10 mol % of both $^{29}SiO_2$ and ZnO, three types of silicate have been detected: (i) SiO_4^{4-} (Q_0 sites) with long longitudinal ($T_{1,Si}$) relaxation times (~10 000 s), which substitute for ~1% of PO_4^{3-}; (ii) silicate nanoinclusions containing Q_2, Q_1, and Q_0 sites with $T_{1,Si} \sim 100$ s, which account for most of the silicon; and (iii) crystalline Q_4 (SiO_2) with long $T_{1,Si}$. Sensitivity was enhanced >100-fold by ^{29}Si enrichment and refocused detection. The inclusions in both samples have a diameter of ~8 nm, as proved by $^{29}Si\{^{31}P\}$ REDOR dephasing on a 30-ms time scale, which was simulated using a multispin approach specifically suited for nanoparticles. ^{29}Si CODEX NMR with 30-s ^{29}Si spin diffusion confirms that an inclusion contains >10 Si (consistent with the REDOR result of >100 Si per inclusion). Overlapping signals of silicate Q_2, Q_1, and Q_0 sites were spectrally edited based on their J-couplings, using double-quantum filtering. The large inhomogeneous broadening of the Q_2, Q_1, and Q_0 ^{29}Si subspectra indicates that the nanoinclusions are amorphous.

(I) Introduction

Among the calcium phosphate ceramics, tricalcium phosphate ($Ca_3(PO_4)_2$, TCP) has been investigated particularly extensively as a promising resorbable bioceramics for bone replacement.[1–3] As a result of its high solubility, it is expected to degrade in the host and be gradually replaced by the regenerating bone, meanwhile serving as a seed of the new bone and a supplier of Ca and PO_4 ions. TCP was reported to be more bioresorbable than hydroxyapatite, which usually shows minimal resorption. However, higher solubility of TCP results in a reduction of the bone-implant strength. Thus, the suitability of TCP for use in vivo is critically dependent on how the dissolution behavior might be controlled by chemical modification.

In our previous research, silicon and zinc were added as stabilizers to modify the dissolution behavior of TCP; these elements are osteoconductive and could stimulate osteogenesis for new bone growth.[4] The previous XRD results showed that TCP doped with 10 mol % Si and Zn at high temperature crystallizes in the low-temperature β-phase. No major secondary or amorphous phase was observed in the diffraction pattern, which indicates that Zn and Si are incorporated into the TCP structure after high temperature sintering. The dissolution study also confirmed that the Zn- or Si-doped TCP is stabilized in simulated body fluid compared with pure TCP.[5] When the doping level is reduced to 5 mol %, some α-TCP signals are observed. Doping only with Si produces α-TCP.[6–8]

The stabilization mechanism was explored from the crystallographic point of view. In the β-TCP unit cell, the Ca(4) and Ca(5) sites are distinct from the other three sites and suitable for smaller cations such as Zn but are highly constrained for Ca^{2+} ions. Ca(4) is on the 3-fold axis and has an unusual coordination to the O(9), O(9′), and O(9″) face of the $P(1)O_4$ group. It has a coordination number of only three, in a flattened tetrahedral configuration, which results in a compressed Ca site. The Ca(4)···O(9) bonds are 3.041(1) Å, longer than the normal Ca···O bond of 2.4 Å. The Ca(5) sites are surrounded by oxygens in a 6-fold distorted octahedral coordination, and all six Ca···O distances are relatively short, in the range of 2.238–2.287 Å.[9,10] Thus, substitution of smaller Zn^{2+} for Ca^{2+} results in a more stable TCP structure by reducing the strain in the structure.

* Corresponding author: e-mail, srohr@iastate.edu; phone, 515-294-6105
† Department of Chemistry.
‡ Department of Materials Science and Engineering.

(1) LeGeros, R. Z.; LeGeros, J. P.; Daculsi, G.; Kijkowaka, R. *Encyclopedia Handbook of Biomaterials Bioengineering*; Marcel Dekker: New York, 1995.
(2) Klein, C. P.; A, T.; Driessen, A. A.; de Groot, K. *Biomaterials* **1984**, *5*, 157–160.
(3) Park, J. B.; Lakes, R. S. *Biomaterials: An Introduction*, 2nd ed.; Plenum Publishing: New York, 1992.
(4) Langstaff, S.; Sayer, M. *Biomaterials* **2001**, *22*, 135–150.
(5) Wei, X.; Akinc, M. In *Ceramic Engineering and Science Proceedings (the 29th International Conference on Advanced Ceramics and Composites - Advances in Bioceramics and Biocomposites)*, Cocoa Beach, FL, 2005; Mizuno, M., Ed.; The American Ceramic Society: Westerville, OH, 2005; pp 129–136.
(6) Reid, J. W.; Tuck, L.; Sayer, M.; Fargo, K.; Hendry, J. A. *Biomaterials* **2006**, *27*, 2916–2925.
(7) Langstaff, S.; Sayer, M.; Smith, T. J. N.; Pugh, S. M.; Hesp, S. A. M.; Thompson, W. T. *Biomaterials* **1999**, *20*, 1727–1741.
(8) Sayer, M.; Stratilov, A. D.; Reid, J.; Calderin, L.; Stott, M. J.; Yin, X.; MacKenzie, M.; Smith, T. J. N.; Hendry, J. A.; Langstaff, S. D. *Biomaterials* **2003**, *24*, 369–382.
(9) Schroeder, L. W.; Dickens, B.; Brown, W. E. *J. Solid State Chem.* **1977**, *22*, 253–262.
(10) Elliott, J. C. *Structure and Chemistry of the Apatites and other Calcium Orthophosphates*; Elsevier: London, 1994.

10.1021/cm702928h CCC: $40.75
Published on Web 03/12/2008

Given the similar tetrahedral structures of PO_4^{3-} and SiO_4^{4-}, P in the TCP structure may be replaced by Si, and substitution of Ca by the smaller Zn also leaves more open space for larger Si substituting in P sites. Our previous Rietveld analysis for lattice parameters and unit-cell volume show an effect of Zn and Si on the crystal structure.[11,12] However, Si may also exist as a secondary phase, which is amorphous or too small in amount to be detected by XRD. Due to limitations in XRD resulting from the similar electron density of Si and P, the details of Si incorporation into TCP are still unclear. Theoretical investigations have been carried out regarding the stability of α- and β-TCP and the fate of silicate ions in a TCP matrix,[13,14] but their predictions of Q_0 sites and Si_2O_7 (Q_1-Q_1) dimers have not been confirmed by experiment.

In this paper, solid-state ^{29}Si and ^{29}Si{^{31}P} nuclear magnetic resonance (NMR) is applied to analyze the Si environment in Si,Zn-doped TCP, to help understand the stabilization mechanism by Si. Modern solid-state NMR provides various methods for characterizing the local structure even of highly complex or disordered solids. ^{29}Si NMR is an excellent means for elucidating structure and chemistry in silicates, which form a rich and varied class of materials including glasses[15,16] and zeolites.[17–19] The local bonding geometry is reflected in isotropic and anisotropic ^{29}Si chemical shifts,[16,19,20] while the number of spins in a cluster can be counted using stimulated-echo experiments, such as CODEX,[21] with ^{29}Si spin diffusion. The present samples were isotopically labeled by ^{29}Si, which greatly enhances sensitivity. In combination with refocused detection,[22,23] a more than 100-fold sensitivity enhancement is achieved. By contrast, earlier routine NMR studies of Si-doped TCP did not yield a ^{29}Si NMR signal.[24] The uniform ^{29}Si labeling also produces homonuclear J-couplings useful for distinguishing different Q_n silicate sites in ^{29}Si−^{29}Si J-modulation or double-quantum experiments and makes ^{29}Si spin diffusion within silicon-rich phases efficient, which enables identification of silicate-rich domains.

The proximity of ^{31}P and ^{29}Si, a crucial observable in Si-doped TCP, can be measured in terms of the strongly distance dependent dipolar couplings between these nuclear spins. In ^{29}Si{^{31}P} rotational echo double resonance (REDOR)[25] experiments, the dephasing rate of the ^{29}Si magnetization reflects the recoupled ^{29}Si−^{31}P dipolar interactions. We present quantitative simulations of REDOR data for nanometer-scale inclusions and demonstrate that although ^{29}Si−^{31}P spin pair dephasing is insignificant for internuclear distances >1 nm, almost complete dephasing can be observed even for nanoparticles of 8-nm diameter.

(II) Experimental Section

Sample Preparation. Commercial reagent-grade $CaCO_3$, $NH_4H_2PO_4$, and ZnO (all from Fisher Scientific, Hampton, NH) were used as received. To increase the signal of the 10- to 20-fold diluted silicon species in the NMR experiments, 99% isotopically enriched $^{29}SiO_2$ (Cambridge Isotope Laboratories, Andover, MA) was used instead of regular unlabeled SiO_2. Because the natural abundance of the NMR-active ^{29}Si isotope of only 4.4%, the isotopic labeling achieves a 23-fold sensitivity gain, reducing the experiment time by a factor of 500. In addition, it results in J-couplings between any two silicon sites connected by oxygen. TCP was synthesized by reacting the appropriate chemical mixture according to the following equation:

$$3CaCO_3 + 2NH_4H_2PO_4 \rightarrow Ca_3(PO_4)_2 + 3CO_2 + 2NH_3 + 3H_2O$$

NMR samples were prepared with 5 mol % and with 10 mol % addition of ZnO and $^{29}SiO_2$. Here, 10 mol % means that the Zn and Si substitutions were 10 mol % of Ca and P (i.e., Si/(Si + P) = Zn/(Zn + Ca) = 0.1). The incorporated amounts of Zn and Si, measured by ICP, were close to the nominal values. The molar ratios of (Zn + Ca):(Si + P) were kept constant at 1.5 as in stoichiometric TCP. The mixture was milled in anhydrous ethanol for 4 h by using alumina milling media. The slurry was vacuum filtered and dried. Thereafter, the powder was sintered at 1300 °C for 10 h in air followed by quenching in dry air. There is no evidence of significant amounts of carbonate introduced from air. Ca and P analysis for a number of samples indicated that the Ca/P ratio ranged between 1.48 and 1.53, clearly within the experimental range for stoichiometric TCP. The wide-angle X-ray diffraction patterns were similar to those of the corresponding materials in ref 12. They show β-TCP peaks, with additional α-TCP signals for the 5%-doped sample. Lattice refinement on neutron powder diffraction data showed that all the Zn is in the TCP structure, mostly substituting for Ca in the Ca(5) sites while a small fraction is added to partially occupied Ca(4); it does not indicate the presence of water in the structure.[11]

NMR parameters. Solid-state NMR experiments were run on a Bruker DSX-400 spectrometer at 162 MHz for ^{31}P and 79 MHz for ^{29}Si. Taking advantage of the very long ^{29}Si transverse relaxation time (T_2) in the system, multiple-echo (CPMG) detection was used for signal enhancement.[22,23] In this scheme, a train of rotation synchronized refocusing 180° pulses are applied on the detection channel (^{29}Si) during acquisition, with detection turned off whenever the refocusing pulse is applied. After Fourier transformation, this produces spikelets whose frequency spacing is the inverse of the time domain spacing of the refocusing pulses. While multiple-echo detection provides a large S/N enhancement, it comes at the cost of loss of some chemical shift resolution, to an extent that depends on the spacing of the refocusing pulses. The refocusing pulses were timed differently depending upon the experimental requirements of signal enhancement or spectral resolution. To prevent sample heating by the long (1.7−6 s) train of refocusing pulses, the duty cycle of the refocusing pulses was kept under 2% and was usually approximately 0.5%, and the 180°

(11) Wei, X.; Akinc, M. *J. Am. Ceram. Soc.* **2007**, *90*, 2709–2715.
(12) Wei, X.; Akinc, M. *Key Eng. Mater.* **2005**, *284–286*, 83–86.
(13) Yin, X.; Stott, M. J. *Phys. Rev. B* **2003**, *68*, 205205.
(14) Yin, X.; Stott, M. J. *J. Chem. Phys.* **2005**, *122*, 027409.
(15) Eckert, H. *Prog. NMR Spectrosc.* **1992**, *24*, 159–293.
(16) Zhang, P.; Dunlap, C.; Florian, P.; Grandinetti, P. J.; Farnan, I.; Stebbins, J. F. *J. Non-Cryst. Solids* **1996**, *204*, 294–300.
(17) Klinowski, J.; Thomas, J. M.; Fyfe, C. A.; Hartman, J. S. *J. Phys. Chem.* **1981**, *85*, 2590–2594.
(18) Fyfe, C. A.; Gies, H.; Feng, Y.; Kokotailo, G. T. *Nature* **1989**, *341*, 223–225.
(19) Epping, J. D.; Chmelka, B. F. *Curr. Opin. Colloid Interface Sci.* **2006**, *11*, 81–117.
(20) Zhang, P.; Grandinetti, P. J.; Stebbins, J. F. *J. Phys. Chem. B* **1997**, *101*, 4004–4008.
(21) deAzevedo, E. R.; Hu, W. G.; Bonagamba, T. J.; Schmidt-Rohr, K. *J. Chem. Phys.* **2000**, *112*, 8988–9001.
(22) Hou, S. S.; Beyer, F. L.; Schmidt-Rohr, K. *Solid State Nucl. Magn. Reson.* **2002**, *22*, 110–127.
(23) Trebosc, J.; Wiench, J. W.; Huh, S.; Lin, V. S. Y.; Pruski, M. *J. Am. Chem. Soc.* **2005**, *127*, 7587–7593.
(24) Langstaff, S.; Sayer, M.; Smith, T. J. N.; Pugh, S. M. *Biomaterials* **2001**, *22*, 135–150.
(25) Gullion, T.; Schaefer, J. *J. Magn. Reson.* **1989**, *81*, 196–200.

pulses were usually set to a "soft" pulse length of 21 μs, which did not decrease their effectiveness.

Magic-angle spinning (MAS) and static ^{29}Si NMR experiments were run in a Bruker double resonance probe head in single-resonance mode. Most single resonance MAS experiments were run at 5 kHz MAS. A variety of recycle delays, up to 90 000 s, were used, with the refocusing pulses spaced at 4.2 ms for an acquisition time t_{aq} = 1.7 s. For selective detection of long-T_1 species, recycle delays of 20 000 s and T_1- filtering times of 1000 s were used.[26,27] The refocusing pulses were spaced at longer intervals of 40 ms, to define the line shape more accurately, with t_{aq} = 5.9 s. Spectral editing was achieved mostly by T_2/J-modulation and by double-quantum filtering (DQF). The T_2/J-modulation was achieved by a simple Hahn echo with echo times 2τ between 80 and 136 ms while the DQF used a refocused INADEQUATE pulse sequence. Recycle delays of 1000 s were used for the T_2/J-modulation experiments to observe Q_0 sites, while 400 s were sufficient for the DQF experiments because of the shorter T_1 of the Q_1 and Q_2 sites. The static homonuclear dephasing experiments were carried out with 5-s recycle delays for the $^{29}SiO_2$ precursor material, while 400-s and 1000-s recycle delays were used for the labeled and unlabeled Si,Zn-doped TCP samples, respectively. The Q_0 sites of the 5% ^{29}Si,Zn-doped TCP were selected by a 20 000-s recycle delay followed by a 1000-s T_1 filter. The refocusing pulses were spaced at 1-ms intervals, with an acquisition time of 80 ms. The CODEX experiments were carried out at 3-kHz MAS with a CODEX recoupling time of one rotation period. The refocusing pulse spacing was 2.7 ms, with t_{aq} = 330 ms.

^{29}Si{^{31}P} REDOR NMR experiments were performed in a 4-mm XYH triple-resonance probe (Bruker Biospin) with a modified tuning insert, at 3 and 6 kHz MAS. The ^{31}P 180° pulse length was 9.4 μs. For improved insensitivity to B_1 inhomogeneity, composite (90°−180°−90°) pulses were used on ^{31}P, while the phase of the single refocusing pulse on the observe channel was varied according to the EXORCYCLE scheme.[28] The composite ^{31}P 180° pulses were optimized in ^{1}H{^{31}P} REDOR experiments on NIST hydroxyapatite (HAp), $Ca_{10}(PO_4)_6(OH)_2$, with detection of the OH protons. HAp was also used as a model system of X{^{31}P} REDOR dephasing of ions homogeneously dispersed in a phosphate, as described in the Supporting Information. The maximum duration of the REDOR dephasing was 80 ms. A total of 32 scans were averaged with a recycle delay of 250 or 400 s. The experiment was first run at 6 kHz MAS and repeated six weeks later at 3 kHz MAS to ensure reproducibility, which turned out to be excellent. During detection, the signal was refocused by a 10- or 20-μs 180° pulse every 1.2 ms, applied 6 kHz off resonance from the signal maximum, for t_{aq} = 1.7 s. This "compressed" the signal into three peaks of ~1 Hz width.

^{29}Si{^{31}P} REDOR Simulations for Silicate Nanoparticles. As a result of the 100% natural abundance of ^{31}P and its relatively large number density of 1/(4.4 nm)^3 in TCP, each ^{29}Si that experiences any significant dipolar coupling to one ^{31}P also sees many other ^{31}P dephasors. Thus, we have to consider an SI_n multispin system. Conveniently, the ^{31}P−^{31}P dipolar couplings are relatively weak, ~2 kHz, and are spun out by MAS. Thus, spin diffusion of ^{31}P z-coherence is slow, and REDOR works.[29]

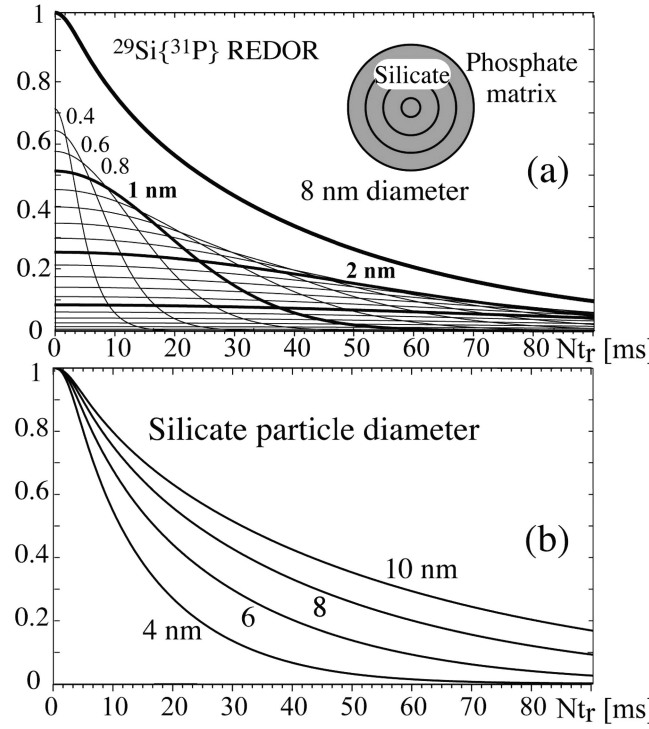

Figure 1. Examples of ^{29}Si{^{31}P} REDOR simulations for spherical silicate particles in a phosphate matrix. (a) Dephasing of different layers, spaced by 0.2 nm. The closest approach of ^{29}Si and ^{31}P is 0.4 nm. The relative intensity corresponds to the number of ^{29}Si in the various shells. Thick line: total dephasing. (b) Total dephasing for various particle diameters.

While the details of REDOR curves in few-spin systems depend on the spatial arrangement of the spins,[30] for nanoparticles the shape of the REDOR curve is dominated by the distribution of distances due to different depths from the interface. As shown in Figure 1, surface and core sites have dramatically different REDOR decay constants. The superposition of the curves corresponding to the different depths z from the silicate−phosphate interface, with shell-volume weighting $p(z)$

$$S(t) = \int_{d_{min}}^{r} S(z, t)\, p(z)\, \mathrm{d}z \qquad (1)$$

produces the "pseudo-exponential" shape observed. Each $S(z, t)$ curve is itself a orientational average (superposition) of the multispin REDOR curves of a ^{29}Si at a given depth. For a multispin system, the initial REDOR decay depends only on the internuclear distances, while the intermediate-time behavior, which often shows low-amplitude oscillations, also reflects the angles between the internuclear vectors.[30] The oscillations interfere away in complex multispin systems. Therefore, we have used Gaussian curves that match the initial behavior correctly. These Gaussians with the second moment $M_2(\theta, z)$ of the REDOR frequencies were calculated for a given depth z and angle θ between a given surface normal and the rotor axis and also depend on the angle γ_0 of the external field B_0 around the rotor axis

$$S(z, t) = \int_0^{2\pi} \int_{-1}^{1} \exp(-M_2(\theta,\gamma_0,z)t^2/2)\, \mathrm{d}\cos\theta \mathrm{d}\gamma_0 \qquad (2)$$

$M_2(\theta, \gamma_0, z)$ is the sum of the squared REDOR frequencies[25,25] of the ^{29}Si−^{31}P spin pairs,

(26) Mowery, D. M.; Harris, D. J.; Schmidt-Rohr, K. *Macromolecules* **2006**, *39*, 2856–2865.
(27) Torchia, D. A. *J. Magn. Reson.* **1978**, *30*, 613–616.
(28) Sinha, N.; Schmidt-Rohr, K.; Hong, M. *J. Magn. Reson.* **2004**, *168*, 358–365.
(29) Schmidt-Rohr, K.; Rawal, A.; Fang, X. W. *J. Chem. Phys.* **2007**, *126*, 054701/054701–054701/054716.
(30) Bertmer, M.; Eckert, H. *Solid State Nucl. Magn. Reson.* **1999**, *15*, 139–152.

$$M_2(\theta,\gamma_0,z) = (0.45)^2(2\pi\mu_0/(4\pi)\gamma_{Si}\gamma_P)^2 \times \sum_n \sin^2(2\beta_n)\sin^2\gamma_n \times 1/r_{SiP,n}{}^6 \quad (3)$$

with β_n, γ_n, and $r_{SiP,n}$ depending on θ and z and γ_n also on γ_0. As in the closely related X{^{1}H} heteronuclear recoupling with dephasing by strong homonuclear interactions of protons (HARDSHIP) NMR simulations,[29] the sum is performed over the ^{31}P spins, which are placed on a cubic lattice with spacing a, which is 4.4 Å in β-TCP according to the density, unit-cell volume, and chemical formula. We can calculate

$$\sin^2(2\beta_n) = 4\cos^2\beta_n(1-\cos^2\beta_n) = 4\{(\mathbf{r}_{rot}\cdot\mathbf{r}_{SiP,n}/r_{SiP,n})^2 - (\mathbf{r}_{rot}\cdot\mathbf{r}_{SiP,n}/r_{SiP,n})^4\} \quad (4)$$

from the dot product cos β_n between the rotor axis $\mathbf{r}_{rot}$ and the ^{29}Si−^{31}P internuclear direction $\mathbf{r}_{SiP,n}/r_{SiP,n}$ and

$$\sin^2\gamma_n = 1-\cos^2\gamma_n = 1-\{(\mathbf{B}_0/B_0\cdot\mathbf{r}_{SiP,n}/r_{SiP,n} - \cos\beta_n\cos(54.7°))/(\sin\beta_n\sin(54.7°))\}^2 \quad (5)$$

from the dot product between the applied magnetic field and the ^{29}Si−^{31}P internuclear direction, $\mathbf{B}_0/B_0\cdot\mathbf{r}_{SiP,n}/r_{SiP,n} = \cos(\theta_{B0,n})$, using $\cos(\theta_{B0,n}) = \cos\beta_n\cos(54.7°) + \sin\beta_n\sin(54.7°)\cos\gamma_n$ with $\cos\beta_n = \mathbf{r}_{rot}\cdot\mathbf{r}_{SiP,n}/r_{SiP,n}$ and $\sin\beta_n = (1-\cos^2\beta_n)^{1/2}$. The Gaussian dephasing curves (not the second moments) for different relative orientations θ of crystallite surface normal and rotor axis and of the B_0 field around the rotor axis (γ_0) are averaged for a given depth z from the interface to produce $S(z, t)$, see eq 2.

How can heteronuclear dipolar couplings, which have a "reach" of <0.8 nm for ^{31}P−^{29}Si spin pairs, probe particles up to 10 nm in diameter? Two reasons can be given: (i) The dephasing of a given ^{29}Si spin by multiple ^{31}P spins (typically $N_P = 40$ for Si far from the interface) in the TCP matrix is $N_P{}^{1/2}$ times faster than in a ^{29}Si−^{31}P spin pair, since $M_2 \sim N_P$. (ii) In a 10-nm diameter sphere, the ∼2-nm thick outer shell that can be dephased significantly within 80 ms (see Figure 1a) accounts for ∼80% of the volume, so significant dephasing (down to ∼20%) will be observed.

(III) Results

^{29}Si Spectra. Figure 2a−d shows various one-dimensional ^{29}Si NMR spectra of 5 and 10 mol % ^{29}Si,Zn-doped TCP. The spectra exhibit significant inhomogeneous broadening of the peaks, which must be due to many different environments. The corresponding large T_2/T_2* ratio is confirmed by sharp lines in spectra obtained with refocused detection, Figure 2d,e. The chemical shifts spread from −68 to −92 ppm, covering the ranges typical of Q_0, Q_1, and Q_2 sites, as well as a Q_4 peak at −110 ppm. Given that Q_4 silicons are linked, via bridging oxygens, to four other silicons, they cannot be associated with the unlinked Q_0 sites. The different $T_{1,Si}$ indicated by the different line shapes in Figure 2a, after 1000 s recycle delays, compared with Figure 2b, after 10 000 s, shows that the Q_4 clusters are not linked to the Q_1 and Q_2 sites.

The different Q_n sites can be distinguished not only by their isotropic chemical shifts but also based on two independent NMR parameters: (i) J-couplings, which increase with n the number of bonded silicon neighbors and (ii) chemical-shift anisotropies, which reflect the local bonding symmetry. While CSAs can be measured without isotopic enrichment, assignment based on the J-couplings requires every silicon to be ^{29}Si, which is true in our fully ^{29}Si-enriched samples. However, before presenting these spectral-editing data, we would like to discuss the $T_{1,Si}$ relaxation times, which reveal three main types of silicate environments.

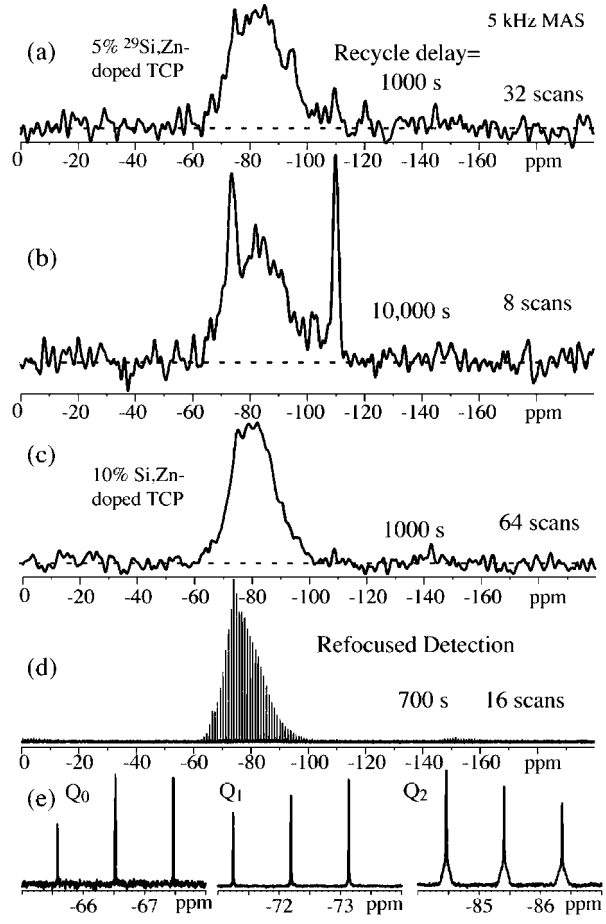

Figure 2. ^{29}Si MAS NMR spectra of 5% and 10% Si,Zn-doped TCP. (a) Regular MAS spectrum of 5% Si,Zn-doped TCP with a 1000-s recycle delay. (b) Same as (a) with 10 000-s recycle delay. (c) Regular MAS spectrum of 10% Si,Zn-doped TCP with a 1000-s recycle delay. (d) Similar to c but with refocused detection for signal enhancement and with a 700-s recycle delay. (e) Expanded views of the spikelets in (d) in the Q_0, Q_1, and Q_2 spectral ranges.

***$T_{1,Si}$* Relaxation Times.** Figure 3 shows ^{29}Si NMR spectra of both ^{29}Si-doped samples, acquired with refocused detection, as a function of recycle delay, from 500 s to 90 000 s. The broad band between −70 and −100 ppm is seen to have a relatively short $T_{1,Si}$ of ∼200 s, while the sharper signals near −70 ppm and −110 ppm exhibit ∼20 times longer relaxation times. This difference is confirmed by 1000-s $T_{1,Si}$-filtered DP spectra with 20 000 s recycle delay, Figure 4, which exhibit only the signals near −70 ppm and −110 ppm. The long $T_{1,Si}$ indicates that these silicates are not in spin-diffusion contact with the other, fast-relaxing silicates. The relatively small inhomogeneous broadening of the peaks near −70 ppm in Figure 4 suggests their origin from specific sites in a crystalline structure, indicating dispersion in TCP. The downfield chemical shift and long $T_{2,Si}$ (no observable J-coupling) of the signals near −70 ppm strongly suggest assignment to Q_0 sites. However, symmetric Q_1−Q_1 dimers, in which chemical equivalence makes the J-coupling undetectable, should also be considered. This will be further discussed below. The sites

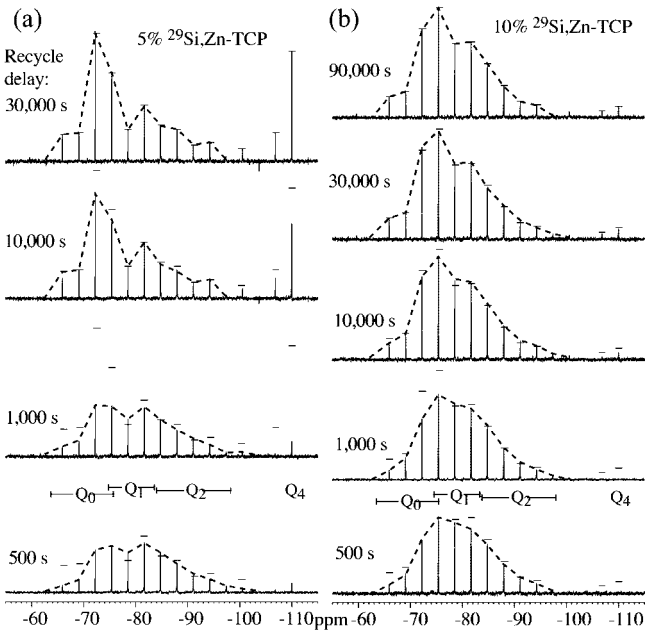

Figure 3. Direct-polarization ^{29}Si MAS NMR spectra of (a) 5% and (b) 10% Si,Zn-doped TCP, acquired with refocused detection, as a function of increasing recycle delays up to 30 000 and 90 000 s, respectively, as labeled. The intensities of the fully relaxed spectrum are indicated by horizontal lines in each spectrum. The ranges of ^{29}Si chemical shifts in Q_n silicate sites given in the literature are indicated above the bottom spectrum. Eight scans were averaged for most of the spectra, except for two with 500-s and 1 000-s recycle delays, where 32 scans were averaged. As a result of the refocused detection, the signal is "compressed" into spikelets. Spinning frequency: 5 kHz.

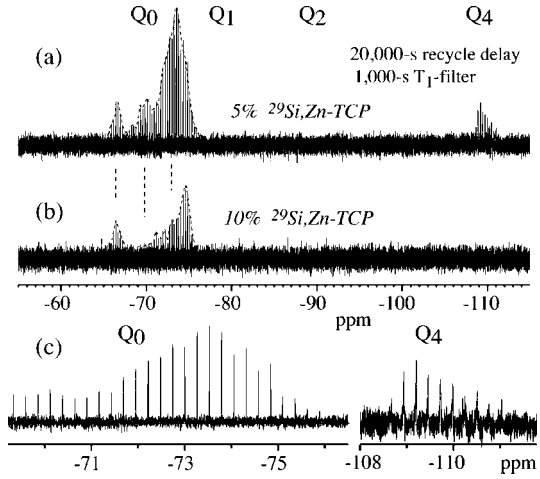

Figure 4. Spectra of the long-$T_{1,Si}$ component, obtained after 1000-s $T_{1,Si}$ filtering and with a 20 000-s recycle delay, acquired using refocused detection with a smaller spacing of spikelets than in Figure 3. (a) 5% ^{29}Si,Zn-doped TCP (20 scans). (b) 10% ^{29}Si,Zn-doped TCP (16 scans). The amount of the 10%-Si,Zn-doped sample was smaller by a factor of 0.43, according to quantitative ^{31}P spectra of the two samples. (c) Expanded views of two spectral ranges of the spectrum in a.

resonating near −110 ppm can be assigned to Q_4 silicates based on their chemical shift. They have six times broader spikelets than the Q_0 sites, see Figure 4c; this homogeneous broadening is due to the J-coupling to their four neighbors; their integrated area for the 5%-Si doped TCP is similar to that of the Q_0 sites, consistent with Figure 2b.

The first and last rows in Table 1 give the fractions of the Q_4 and dispersed Q_0 silicate, respectively, in the two samples studied. The long $T_{1,Si}$ makes a detailed characterization of these crystalline silicate sites extremely time-consuming. Nevertheless, measurements of the J-couplings and dipolar couplings of the Q_0 sites will be presented below, and CSA measurements are shown in the Supporting Information.

Table 1. Quantification of Q_n Silicate Sites in the Two Si,Zn-Doped TCP Samples Studied, Based on Long-Recycle-Delay Spectra and Spectral Editing

type of silicate site	5% ^{29}Si,Zn-TCP	10% ^{29}Si,Zn-TCP	error margins
Q_0 dispersed	16%	12%	±4%
Q_0 in inclusions	4%	5%	±4%
Q_1 in inclusions	25%	45%	±5%
Q_2 in inclusions	35%	35%	±3%
Q_4	20%	3%	±2%

Assignment of Q_n Sites by J-Couplings. The number of J-couplings experienced by a ^{29}Si nucleus strongly affects its spin dynamics. This differential behavior enables us to obtain spectra predominantly of Q_2, Q_2-Q_1, Q_1-Q_1, and Q_0 sites in the ^{29}Si-enriched samples. The J-couplings between two ^{29}Si spins across a bonding oxygen is 3–8 Hz, requiring evolution for $\tau = 1/(2J)$ between 160 and 60 ms for maximum double-quantum signal generation. Conversely, a ∼100-ms J-modulation period in a Hahn spin–echo experiment, where chemical-shift (and heteronuclear) dephasing is refocused but J-modulation continues throughout, results in dephasing first of Q_2 and then of Q_1 signals. Q_0 sites dephase only slowly because they experience no J-couplings and the residual homonuclear dipolar couplings are also very small. Another type of site that would dephase slowly is symmetric Q_1-Q_1 dimers, in which the two silicons are chemically equivalent. More typically Q_1 sites are modulated by $\cos(\pi J 2\tau_1)$, Q_2 sites by $\cos^2(\pi J 2\tau_1)$. The full initial J-modulation curves are shown in Figure 6d below.

In a double-quantum (DQ) filtered spectrum, the signal is proportional to the double-quantum coherence of two coupled spins generated during the excitation period τ_{DQ}. The excitation occurs due to homonuclear J-coupling, potentially aided by residual dipolar couplings. For short times, the spin-pair approximation is valid and the signal contribution from each partner in a pair is equal. For instance, a Q_1-Q_2-Q_1 trimer would be considered as a superposition of a Q_1-Q_2 and a Q_2-Q_1 spin pair, and the Q_2:Q_1 signal ratio would be 1:1, even though there are twice as many Q_1 spins. In other words, due to its two J-couplings, a Q_2 site exhibits a twice faster initial build-up of DQ coherence compared to the Q_1 sites. The differential enhancement of the Q_2 signals in Figure 5i,j appears to be even more pronounced, suggesting that the Q_2-Q_2 J-coupling is larger than the Q_2-Q_1 coupling, which in turn is larger than the effective Q_1-Q_1 coupling.

At longer DQ excitation plus reconversion times of 2·120 ms, Figure 5k,l, the Q_2 signals are quickly dephased, since a Q_2 silicon is part of a system of three or more coupled spins, and the spins outside the DQ spin pair dephase the DQ coherence within 1/(2J). In contrast, the Q_1 signals grow in intensity due to the longer DQ excitation. At longer times, an even more downfield part of the spectrum grows further in intensity, see Figure 5m,n. This must be assigned to Q_1-Q_1 dimers, which are ideal spin pairs unaffected by couplings to a third spin. Their relatively slow rise (no signal at −72 ppm is visible after 40 ms) supports our hypothesis that the

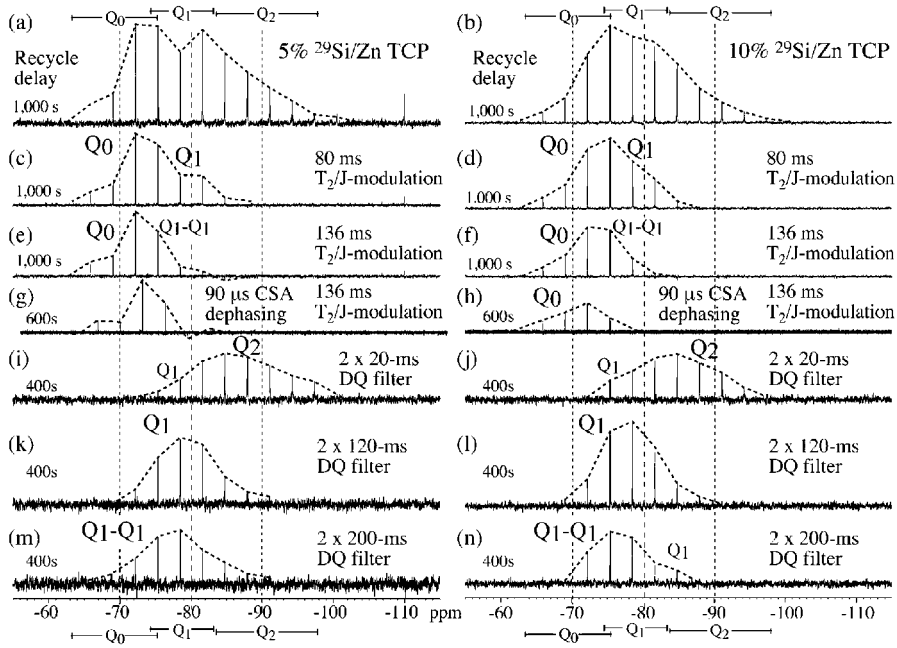

Figure 5. Spectral editing of silicate Q_n species in ^{29}Si NMR based mostly on J-couplings, for the 5%- and 10% Si,Zn-doped TCP (left and right column, respectively). Spectra were obtained at 5 kHz MAS with refocused detection of ~1-s duration. Peaks are connected by a dashed line, which gives the outline of the regular spectrum. The subspectra have been scaled vertically to roughly match their contribution to the spectra in (a) and (b). Major contributions are indicated in larger, minor residual ones in smaller font. (a, b) Almost full spectra obtained with 1000-s recycle delay; the downfield signal of Q_0 sites is not fully relaxed (see Figure 2). (c,d) Spectra after 80 ms of T_2 relaxation/J-modulation, suppressing the signal of Q_2 sites. (e, f) Spectra after 136 ms of T_2 relaxation/J-modulation, suppressing the signal of Q_2 and certain Q_1 sites. (g, h) Spectra after 136 ms of T_2 relaxation/J-modulation and a 90-μs CSA filter, suppressing the Q_1 signals more extensively. (i, j) Spectra after short DQ filter of 4*10 ms, producing a strong Q_2-site signal due to the two J-couplings of these sites, and a weak Q_1-signal contribution. (k, l) Spectra after longer DQ filter of 4*60 ms, producing a strong Q_1-site signal while the Q_2 signal is suppressed by the multiple J- and dipolar couplings of Q_2 sites. (m, n) Spectra after a long DQ filter of 4*100 ms, producing a strong Q_1-site signal that is probably dominated by Q_1–Q_1 dimers. For the spectra in (b−n), between 32 and 128 scans were averaged.

effective J-couplings between two Q_1 sites (i.e., in a dimer) are weaker than those involving Q_2 sites.

Quantification of Q_n Species. By matching signals in the spectrally edited spectra of Figure 5 to the quantitative spectra after long recycle delays and recording the appropriate integrals, the fractions of silicate Q_n sites can be quantified. First of all, on the basis of the comparison of the spectra with 1000 s and 30 000 s recycle delays in Figure 3, the fraction of dispersed long-$T_{1,Si}$ Q_0 sites was determined. Scaling the CSA and T_2/J filtered spectra (Figure 5g,h) to match the Q_0 signal on the downfield side of the DP spectrum with t_{rec} = 1000 s gives an estimate of the fast relaxing Q_0 sites. Scaling the 2*20 ms DQ spectrum (Figure 5i,j) to match the right-hand side of the DP spectrum for t_{rec} = 30 000 s, where there is no overlap with other signals, gives the fraction of Q_2 sites. Scaling the 2*120 ms DQ spectrum (Figure 5k,l) to match the Q_1 sites in the DP spectrum for t_{rec} = 1000 s gives a lower limit to the fraction of Q_1 sites. The resulting peak integrals and error margins for both samples are summarized in Table 1. The Q_2 fraction dominates in the 5%-doped sample; this is not fully obvious from the signal height in the refocused spectra because of the larger homogeneous width of the Q_2 spikelets (see Figure 2e for an extreme example due to long delays between refocusing pulses), which is due to J- and residual dipolar couplings. The larger Q_1 fraction in the 10%-doped sample is confirmed by direct inspection of the spectra in Figures 2, 3, and 5.

^{31}P−^{29}Si Proximity from REDOR. Is all of the silicate, not just the long-$T_{1,Si}$ component resonating near −70 ppm, really dispersed in the TCP matrix? This question can be answered convincingly by ^{29}Si{^{31}P} REDOR NMR, which can probe silicate inclusions between 0.4 and 10 nm in diameter, as discussed above. Figure 6 shows ^{29}Si{^{31}P} REDOR data obtained on the ^{29}Si-labeled sample. They were obtained with recycle delays of 250 s that yield strong signals of the short-$T_{1,Si}$ component but not of the dispersed-silicon long-$T_{1,Si}$ component. When the coupling of the ^{29}Si to the ^{31}P spins is "switched on" by one 180° pulse per half-rotation period, the magnetization of the ^{29}Si spins is dephased on a time scale that is the inverse of the ^{31}P−^{29}Si dipolar coupling. On the one hand, the observed dephasing of ^{29}Si by ^{31}P to <10% proves that more than 90% (probably all) of the silicon is in the proximity of the phosphate matrix. Given that the ^{31}P−^{29}Si dipolar couplings become negligible for distances >3 nm, the silicate must be dispersed on a nanometer scale. On the other hand, the dephasing is slower than expected for individual silicate ions dispersed in the calcium phosphate matrix. We have used OH^- ions in hydroxyapatite as a reference for ions dispersed in a phosphate matrix, with a distance between OH^- protons and the nearest ^{31}P of around 0.4 nm (see also Supporting Information). Figure 6a shows that the γ_H/γ_{Si}-scaled dephasing of the hydroxide protons by ^{31}P (triangles and circles) is 10 times faster than that of ^{29}Si in doped TCP (squares); the hydroxyapatite data were fit by dephasing by three ^{31}P spins at a 0.4-nm distance. This large difference in dephasing time constants can only be explained by clustering of the silicate. The quantitative REDOR fitting procedure for nanoparticles described above matches the data well; see the

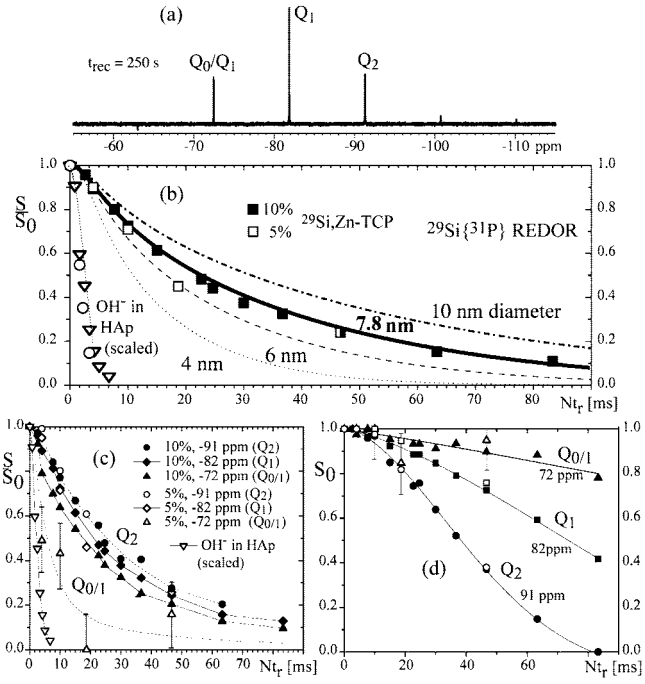

Figure 6. $^{29}Si\{^{31}P\}$ REDOR data of 5% and 10% ^{29}Si,Zn-doped TCP at 3 and 6 kHz MAS. (a) ^{29}Si S_0 spectrum consisting of three spikelets (at –72, –82, and –91 ppm, that is, spaced by 3 kHz/4) produced from the inhomogeneously broadened spectrum by refocused detection, which enhances the sensitivity by an order of magnitude. (b) Dephasing of the total ^{29}Si intensity. Simulated REDOR curves for spherical silicate particles of 4–10 nm diameter are shown for reference. $^{1}H\{^{31}P\}$ REDOR dephasing of OH protons in NIST hydroxyapatite, recorded in the same probehead with identical ^{31}P pulses (see Supporting Information), is also shown (open circles and triangles). This shows the decay expected for isolated ions in a phosphate matrix (three ^{1}H-^{31}P nearest-neighbor distances of 0.4 nm). For a meaningful comparison with the $^{29}Si\{^{31}P\}$ REDOR dephasing, the $^{1}H\{^{31}P\}$ dephasing time has been scaled by $\gamma_H/\gamma_{Si} = 5$, and the data were recorded at 12-kHz MAS, which results in a 4-fold increase in the number of dephasing pulses compared to 3-kHz MAS. In addition, open circles mark $^{1}H\{^{31}P\}$ REDOR dephasing for 10 t_r with a 5-fold reduction of the effective REDOR dephasing frequency by four refocusing π-pulses on ^{1}H, recorded at 3-, 4.5-, and 6-kHz MAS. (c) Dephasing of the three sharp ^{29}Si spikelets in (a). (d) Dephasing of S_0 for the three spikelets shown in (a).

bold fit curve in Figure 6a, for spherical inclusions of 7.8-nm diameter. Note, however, that NMR cannot determine the shape of the inclusions reliably; various inclusion shapes with similar surface/volume ratios will produce acceptable fits.[29]

The data for the 5% and 10% ^{29}Si,Zn-doped TCP are quite similar. The only exception is again associated with a fraction of the upfield signal from the 5%-doped sample, which is dephased quickly by ^{31}P; see the curve of the −72-ppm peak in Figure 6b. This indicates that these ions are dispersed in the phosphate matrix. These are clearly the Q_0 sites identified in the J-modulation experiments. Note that the strongly differential "T_2" behavior (J-modulation) of the S_0 signals plotted in Figure 6c confirms that the three peaks, from right to left, are dominated by Q_2, Q_1, and $Q_1 + Q_0$ sites, respectively.

In these REDOR experiments, the ^{29}Si isotopic labeling was necessary to increase the sensitivity, about 22-fold, but this barely compensates for the 10- or 20-fold dilution of the SiO_2 in the calcium phosphate matrix. Further signal enhancement by refocused detection was crucial for making the REDOR experiments feasible within an acceptable time

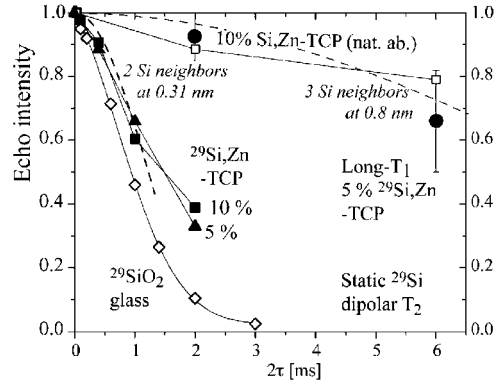

Figure 7. ^{29}Si homonuclear dipolar dephasing (T_2) data of 5% and 10% Si,Zn-doped TCP (filled triangles and squares, respectively), acquired without sample rotation and with refocused detection. Filled circles are data points for the long-$T_{1,Si}$ Q_0 component selected by a 1000-s $T_{1,Si}$ filter after a 20 000-s recycle delay. Data for the unlabeled 10% Si,Zn-containing TCP (i.e., with 4% ^{29}Si, open squares) and for ^{29}Si-labeled SiO_2 (mostly Q_4 sites, open diamonds) are shown for comparison. Two dashed parabolic fit curves based on a short-time (second-moment) approximation are shown: fast dephasing by two ^{29}Si neighbors at 0.31 nm as typical for Q_2 sites in a silicate and slow dephasing by three ^{29}Si neighbors at 0.8 nm.

frame, as a result of the large (inhomogeneous) line broadening and because the 4-mm triple-resonance probe head used for REDOR has a five times smaller sensitivity than the 7-mm double-resonance probe head used for single-resonance ^{29}Si NMR.

Clustering of Silicate: Homonuclear T_2. The ^{29}Si labeling enables us to confirm the clustering of silicates in inclusions. Since every silicon site contains the NMR-active nuclear magnet ^{29}Si, close proximity of silicons can be detected in terms of homonuclear dipolar couplings. The number of nearest neighbors can be estimated based on quantitative analysis of homonuclear T_2 relaxation data, measured in a simple Hahn-echo experiment with multiple-echo detection for sensitivity enhancement. The ^{29}Si 180° pulse refocuses all heteronuclear couplings (e.g., to ^{31}P) and chemical shifts. Without sample rotation, the dominant T_2 mechanism is the $^{29}Si-^{29}Si$ homonuclear dipolar coupling. Thus, the T_2 decay reflects the second moment of the $^{29}Si-^{29}Si$ dipolar couplings.

Figure 7 shows the dipolar T_2 decays of various silicate species. The curve of the $^{29}SiO_2$ precursor material traces out the relaxation behavior of silicon sites completely surrounded by homonuclear neighbors. The resulting curve, which can be fit by a Gaussian,[31] quite closely resembles the short-time behavior of the ^{29}Si dipolar T_2 curve of 10% Si,Zn-doped TCP, indicating that in the latter many ^{29}Si sites are indeed almost completely surrounded by other ^{29}Si. A model system with random placement of 4.4% ^{29}Si is provided by unlabeled fused silica (SiO_2). Its slow decay matches that of the long-$T_{1,Si}$ Q_0 signal (filled circles), which confirms that these are dispersed SiO_4^{4-} ions in the phosphate matrix. The slow dipolar dephasing proves that these are not symmetric Q_1-Q_1 dimers, as produced in a simulation of silicon in TCP.[14] While the transverse magnetization of such chemically equivalent silicon sites would commute with the $\mathbf{I}\cdot\mathbf{J}$ operator in the J-Hamiltonian and

(31) Wu, Y.; Ackerman, J., L.; Kim, H.-M.; Rey, C.; Barroug, A.; Glimcher, M. *J. Bone Miner. Res.* **2002**, *17*, 472–480.

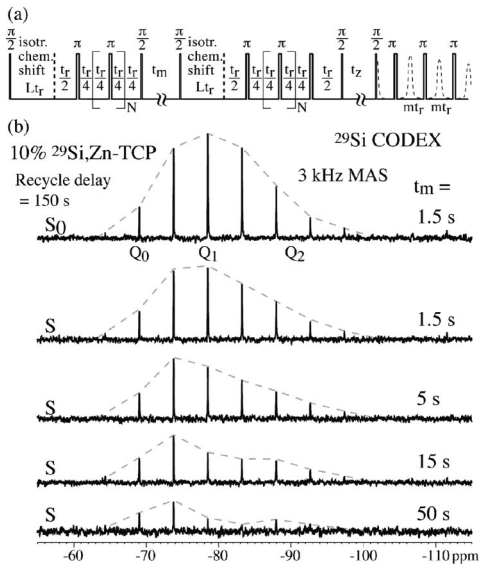

Figure 8. Counting silicates in clusters by CODEX ^{29}Si NMR with ^{29}Si spin diffusion during mixing times of up to 50 s, for 10% Si,Zn-doped TCP. (a) Pulse sequence to generate not only an anisotropic chemical-shift stimulated echo as in standard CODEX but also an isotropic chemical-shift stimulated echo. (b) Series of spectra after CODEX with the spin-diffusion time t_m given on the right. The spectra have been scaled up to eliminate the effects of $T_{1,Si}$ relaxation during the mixing time t_m.

therefore show no J-modulation, it would not commute with the additional $3I_zJ_z$ term in the dipolar coupling and therefore be subject to fast homonuclear dipolar dephasing.

Counting ^{29}Si Spins in Clusters by CODEX NMR. A lower limit to the number of ^{29}Si spins in an inclusion can be obtained by stimulated-echo measurements with spin ^{29}Si diffusion. If during a "mixing time" t_m the magnetization has diffused to a ^{29}Si spin of different chemical shifts, the contribution to the stimulated echo will be negligible if the dephasing/rephasing periods Nt_r are long enough. In other words, only the magnetization that remains on the initially polarized spin contributes to the stimulated echo. If there are M spins in a cluster, at long spin-diffusion times only $1/M$ of the magnetization contributes to the stimulated echo.[21]

The CODEX experiment enables stimulated-echo measurements under MAS even for chemically equivalent sites.[21] The pulse sequence of Figure 8a is modified from the standard CODEX experiment in that it contains not only recoupled anisotropic chemical shift but also isotropic-shift evolution and reconversion periods. Thus, dephasing occurs as a result of a change not only in anisotropic but also in isotropic chemical shift. Figure 8b shows a series of ^{29}Si spectra of the 10% Si,Zn-doped TCP, obtained after CODEX with spin diffusion for times t_m ranging between 1.5 and 50 s. The intensity of the Q_1 and Q_2 signals decreases by a factor of up to 10, proving that each cluster contains at least $M = 10$ distinguishable (magnetically inequivalent) silicon sites. The Q_0 signal also decreases, proving that the inclusions contain some Q_0 sites. The slower dephasing of the signals near -70 ppm is most likely due to contributions from some of the SiO_4^{4-} ions dispersed in the TCP matrix.

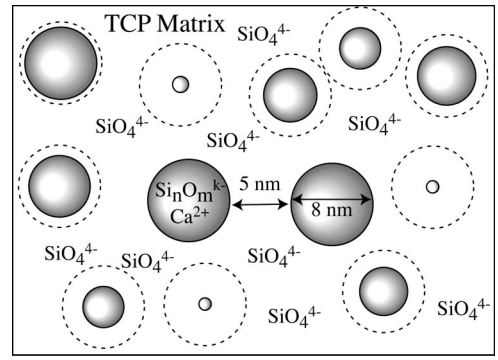

Figure 9. Structural model of 10% Si,Zn-doped TCP on the nanometer scale, with silicate ions dispersed in the TCP matrix (Q_0 sites) indicated by SiO_4^{4-} and spherical silicate clusters. An idealized cross section is shown. Note that many particles are not sliced through their center and therefore appear smaller than their full 8-nm diameter. For reference, the maximum outlines of the particles are shown by dashed circles.

(IV) Discussion

The spectroscopic and relaxation time analysis has revealed three distinct silicate components: (i) Long-$T_{1,Si}$ Q_0 silicate tetrahedra dispersed in TCP; (ii) short-$T_{1,Si}$ Q_2, Q_1, and Q_0 sites in clusters that form inclusions in the TCP matrix; and (iii) long-$T_{1,Si}$ Q_4 crystallites. Figure 9 shows a schematic of the morphology of components (i) and (ii) on the 20-nm scale. $T_{1,Si}$ and connectivity analysis shows that the Q_4 component (iii) is not in close contact with the other two components.

Dispersed Q_0 Sites. SiO_4^{4-} ions (Q_0 sites) dispersed in the TCP matrix have been identified by long $T_{1,Si}$ relaxation times, lack of J-modulation, a downfield chemical shift, sharp resonances, and a small chemical-shift anisotropy. Symmetric Q_1-Q_1 dimers, which would also show no J-modulation due to chemical equivalence, are excluded by the long dipolar T_2. Note that dispersed Q_0 sites that happen to be located near a silicate inclusion will have homonuclear couplings with the clustered silicate and therefore have a shortened $T_{1,Si}$. This may result in some of the dispersed Q_0 sites being counted incorrectly as belonging to the silicate inclusions.

The absolute concentration of dispersed silicate ions relative to phosphate ions is similar in both samples, 0.8 mol % and 1.2 mol % Si in the 5%- and 10%-doped samples, respectively. This should be compared with a value of 3.9 mol % estimated from neutron-scattering Rietveld analysis on a similar (but not identical) TCP sample with 10% Si,Zn doping.[11] We cannot exclude categorically that the true fraction of dispersed SiO_4^{4-} ions is larger than estimated by NMR, if that component has an unusually long $T_{1,Si}$ relaxation time $>90\,000$ s. Note that in spite of similar absolute amounts of dispersed Q_0 sites, their sharp peaks are less visible in the spectra of the 10% ^{29}Si,Zn-doped sample because they represent a smaller fraction of silicon.

According to neutron diffraction refinement data, the Si substitutes exclusively for P(1) at location (0,0,0) in the A column of the β-phase of TCP.[11] The fact that multiple peaks of the Q_0 sites are observed in NMR, see Figure 4, casts doubt on that interpretation, but more detailed investigations, for instance by ^{29}Si$-^{31}$P NMR, would be extremely time-consuming because of the long T_1 relaxation times and low concentration of Q_0 sites.

Silicate Nanoinclusions. NMR and neutron scattering agree that the majority (>60%) of the silicate does not substitute for phosphate in the TCP crystal lattice. Our NMR study has identified the silicate that is "invisible" to neutron scattering as forming 8-nm diameter silicate inclusions containing a variety of Q_2, Q_1, and Q_0 sites. $^{29}Si\{^{31}P\}$ REDOR, ^{29}Si CODEX, and dipolar ^{29}Si T_2 consistently show the silicate clustering. This component exhibits a relatively short, uniform $T_{1,Si}$, which is further evidence that all these silicate sites are in spin-diffusion contact with each other and not separated by the phosphate matrix. REDOR provides the most useful information on the composition and size of the inclusions, 7.8 ± 0.5 nm in both samples. The slow dephasing proves that this component does not contain phosphate. On the other hand, the ^{29}Si magnetization does dephase to less than 10% after 80 ms of ^{31}P recoupling, which proves that essentially all silicate is dispersed in the phosphate.

The three methods give consistent estimates of the cluster size. The most specific information comes from the REDOR measurements, which show that an inclusion is typically 7.8 nm in diameter and thus contains >100 silicons. Dipolar T_2 only confirms that each silicon is surrounded by several other silicons. CODEX shows that at least 10 ^{29}Si interact within a 50-s mixing time; longer mixing times could in principle reveal larger numbers but were precluded by $T_{1,Si}$ relaxation. Spherical inclusions on a similar size scale as indicated by NMR have been detected in a TEM micrograph of a related sample, 3% Si,Zn-doped TCP. [32]

The pronounced inhomogeneous broadening of the ^{29}Si band indicates that the inclusions are most likely amorphous. This is also supported by the somewhat different proportions of Q_2, Q_1, and Q_0 sites for the two samples studied (see Table 1), which would not occur for a single however complex crystalline structure. This difference is indicated directly by somewhat different intensity distributions in the spectra of the two samples, see Figure 2a versus 2c and Figure 3a versus 3b. Note that the Q_2- and Q_1-rich calcium silicate structure of the inclusions is completely different from the amorphous $^{29}SiO_2$ starting material, where almost all sites are Q_4. The inclusions are shown as spherical in the schematic of Figure 9. This is a conjecture, given that the NMR data do not provide reliable information on particle shape but reflect mostly the surface-to-volume ratio.[29]

This study demonstrates that NMR can detect amorphous nanoinclusions that are practically invisible to scattering methods. It is conceivable that such nanoparticles also exist in other ceramics that have only been studied by scattering methods and that they may affect mechanical properties such as hardness or toughness.

(32) Wei, X. Ph.D. Thesis, Materials Science & Engineering, Iowa State University, Ames, IA, 2006.

Q_4 Silicate Species. Signals of Q_4 silicates at −110 ppm are seen on both samples but more prominently in the 5% doped sample. The significantly different mole fraction in the two samples confirms that this component is unrelated to the two others. Their long T_1 compared to the Q_1 and Q_2 sites further corroborates this conclusion. It also proves that these Q_4 components are not simply residual fused-silica starting material, which has a T_1 of only a few seconds. The line width of only ±2 ppm, see Figure 4a and 2b, is also smaller than that of fused silica (±6 ppm). The Q_4 silicates could be bonded to either phosphate or other silicates. The strong loss of intensity of the Q_4 spikelet after a 80 ms T_2/J filter, see Figure 5c, and the large line-broadening due to homonuclear J-couplings, see Figure 4c, strongly suggests silicate neighbors. This is corroborated by the $^{29}Si\{^{31}P\}$ REDOR dephasing of the small spikelet mostly of the Q_4 sites, which is not nearly as fast as that of the dispersed Q_0 sites. In summary, the data suggest a crystalline Q_4 phase such as cristobalite.

For both 5 and 10% Si,Zn-doped TCP, neutron scattering indicated that all of the Zn ions occupy the Ca sites in the TCP structure, while only a minority fraction of the Si substitutes for the P sites as shown by both neutron scattering and NMR. NMR also showed that the remaining Si is in the form of ~8 nm silicate clusters that are distributed in the TCP matrix. The fact that these samples were synthesized at 1300 °C for 10 h suggests that the presence of such clusters is not due to kinetic limitations but rather due to limited solubility of Si in TCP. A previous study in our group found a dramatic reduction in the solubility of the TCP in simulated body fluid by the addition of small amounts of Si.[5] However, whether this reduction is due to Q_0 sites or nanoclusters, or both, is not clear at this point.

Outlook. The insights into the nature and relaxation times of the different components in the ^{29}Si NMR spectrum obtained here enables ^{29}Si NMR, even without isotopic labeling but using refocused detection, to be used to monitor the state of Si in TCP. In dissolution studies guided by NMR, processing conditions could be varied to identify and then enhance the component that optimizes the dissolution behavior of TCP for its application as a bone-replacement material.

Acknowledgment. Work at the Ames Laboratory was supported by the Department of Energy-Basic Energy Sciences (Materials Chemistry and Biomolecular Materials Program) under Contract No. DE-AC02-07CH11358.

Supporting Information Available: The calibration of $X\{^{31}P\}$ REDOR by means of $^{1}H\{^{31}P\}$ REDOR of hydroxyapatite and the measurement of chemical shift anisotropy dephasing, which supports the assignment of the Q_n sites, are described (PDF). This material is available free of charge via the Internet at http://pubs.acs.org.

CM702928H